

# Ferroelectricity driven by the non-centrosymmetric magnetic ordering in multiferroic TbMn<sub>2</sub>O<sub>5</sub>: a first-principles study

Chenjie Wang, Guang-Can Guo, and Lixin He\*

Key Laboratory of Quantum Information, University of Science and Technology of China, Hefei, 230026, People's Republic of China

(Dated: October 25, 2018)

The ground state structural, electronic and magnetic properties of multiferroic TbMn<sub>2</sub>O<sub>5</sub> are investigated via first-principles calculations. We show that the ferroelectricity in TbMn<sub>2</sub>O<sub>5</sub> is driven by the non-centrosymmetric magnetic ordering, without invoking the spin-orbit coupling and non-collinear spins. The *intrinsic* electric polarization in this compound is calculated to be 1187 nC·cm<sup>-2</sup>, an order of magnitude larger than previously thought.

PACS numbers: 75.25.+z, 77.80.-e, 63.20.-e

Multiferroics with magnetic and electric ordering united in a single phase were thought to be rare[1, 2]. Surprisingly, a large class of manganese oxides (RMnO<sub>3</sub> [3, 4], and RMn<sub>2</sub>O<sub>5</sub> [5, 6, 7] with R=Y, Tb, Dy, etc.) has recently been discovered to be multiferroic. Unlike the traditional multiferroics where the two order parameters only couple weakly[1], the newly discovered materials possess strong magnetoelectric (ME) coupling, resulting in various novel physical effects. One of the most prominent examples is given by TbMn<sub>2</sub>O<sub>5</sub>[5, 8], which displays clear correlated anomalies of the dielectric constant  $\epsilon$  with the spin ordering [5]. More strikingly, the electric polarization in this material can be reversed by applying a magnetic field [5]. The remarkable ME effects revealed in these materials have attracted great attention [1, 3, 4, 5, 6, 7, 8, 9, 10, 11, 12] because of the fascinating physics and their potential applications in novel multifunctional ME devices.

Although great effort has been devoted to understanding the fundamental mechanism of the giant ME coupling, our knowledge of the manganese oxide multiferroics is still very limited and full of puzzles. For example, experimental data show that the structure of TbMn<sub>2</sub>O<sub>5</sub> has space group *Pbam* [13], which includes spatial inversion ( $R^{-1}$ ) symmetry. It is therefore puzzling that the compound develops spontaneous electric polarizations. It has been suspected [6, 9] that the actual symmetry group of TbMn<sub>2</sub>O<sub>5</sub> is *Pb2<sub>1</sub>m*, allowing polarizations. Indeed, there are several experiments supporting this hypothesis [6, 7, 10]. Nevertheless, no *direct* evidence of the lower symmetry has yet been found [6, 7]. Theoretically, the origin of the giant ME coupling and the ferroelectricity in these materials is still under intensive debates [6, 8, 11, 12]. One of the fundamental questions that remain unsolved is whether the spin-orbit interaction [11, 12] is essential for the ME coupling and ferroelectricity in these materials.

In this letter, we carry out a first-principles study of TbMn<sub>2</sub>O<sub>5</sub>, to identify its crystal structure and clarify the microscopic origin of the ferroelectricity. We compute physical quantities that can be directly compared to the experiments. To the best of our knowledge, no such study has yet been done for TbMn<sub>2</sub>O<sub>5</sub> (and other RMn<sub>2</sub>O<sub>5</sub> compounds [7]), because it has very complicate incommensurate anti-ferromagnetic (AFM) structure with the propagation vector  $\mathbf{k} \approx (0.48, 0, 0.32)$ . To accommodate the magnetic structure, one needs a huge supercell, which is computationally prohibitive. Instead, we use a  $2 \times 1 \times 1$  supercell, equivalent to approximating the propagation vector  $\mathbf{k} = (0.5, 0, 0)$ . The validity of this approximation will be justified later in the text. Our results show that the ferroelectricity in TbMn<sub>2</sub>O<sub>5</sub> is driven by the non-centrosymmetric magnetic ordering and the asymmetric exchange interactions, without invoking the spin-orbit coupling and non-collinear spins. The *intrinsic* electric polarization in this compound is calculated to be 1187 nC·cm<sup>-2</sup>, much larger than previously thought for this type of compound [1, 5].

The calculations are based on the density functional theory (DFT) within the spin-polarized generalized gradient approximation (GGA) [14] implemented in the Vienna *ab initio* Simulations Package (VASP) [15, 16]. The projector augmented-wave (PAW) pseudopotentials [17] with a 500 eV plane-wave cutoff are used. A  $1 \times 2 \times 4$  Monkhorst-Pack k-points mesh converges very well the results. We use the collinear spin approximation without the spin-orbit coupling. Our results agree very well with the known experiments, indicating that these approximations capture the essential physics in TbMn<sub>2</sub>O<sub>5</sub>.

The crystal structure of TbMn<sub>2</sub>O<sub>5</sub> is orthorhombic, with four TbMn<sub>2</sub>O<sub>5</sub> formula units (32 atoms in total) per primitive cell, containing Mn<sup>4+</sup>O<sub>6</sub> octahedra and Mn<sup>3+</sup>O<sub>5</sub> pyramids [13]. We relax the crystal structure beginning with the experimental structural parameters[13], listed in Table I. The most stable structure we found has the spin configuration identical to that was proposed in Ref. 6, as illustrated in Fig. 1(a). It also has an energetically degenerate structure, shown in Fig.

\*corresponding author, Email address: helx@ustc.edu.cn

TABLE I: Comparison of the calculated and measured structural parameters of  $\text{TbMn}_2\text{O}_5$ . The lattice constants are given in  $\text{\AA}$ . Atoms that occupy the same Wyckoff positions are shown only once.

	Theory ( $Pb2_1m$ )			Experiment ( $Pbam$ )		
	$a$	$b$	$c$	$a$	$b$	$c$
$a, b, c$	7.3014	8.5393	5.6056	7.3251	8.5168	5.6750
$\text{Tb}^{3+}$	0.1410	0.1733	0	0.1399	0.1726	0
$\text{Mn}^{4+}$	0.0001	0.5003	0.2558	0	0.5	0.2618
$\text{Mn}^{3+}$	0.4012	0.3558	0.5	0.4120	0.3510	0.5
$\text{O}_1$	0.0008	0.0002	0.2709	0	0	0.2710
$\text{O}_2$	0.1645	0.4480	0	0.1617	0.4463	0
$\text{O}_3$	0.1560	0.4329	0.5	0.1528	0.4324	0.5
$\text{O}_4$	0.3977	0.2077	0.2438	0.3973	0.2062	0.2483
	0.8959	0.2919	0.7579			

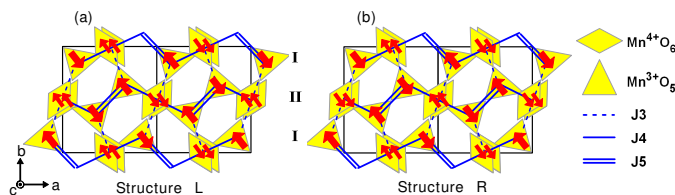


FIG. 1: (Color online) The ground state spin configurations for two energetically degenerate structure  $L$  and  $R$ . The diamonds and triangles denote the  $\text{Mn}^{4+}\text{O}_6$  octahedra and  $\text{Mn}^{3+}\text{O}_5$  pyramids respectively. The dashed, single and double lines represent  $J_3$ ,  $J_4$  and  $J_5$  exchange interactions respectively, following Ref. 6.

1(b). We denote the two structures “left” ( $L$ ) and “right” ( $R$ ) respectively. In these magnetic structures,  $\text{Mn}^{4+}$  form an AFM square lattice in the  $ab$  plane, whereas  $\text{Mn}^{3+}$  couples to  $\text{Mn}^{4+}$  either antiferromagnetically via  $J_4$  along  $a$  axis or with alternating sign via  $J_3$  along  $b$  axis.  $\text{Mn}^{3+}$  ions in two connected pyramids also couple antiferromagnetically through  $J_5$ . Here, we adopt the notations  $J_3$ ,  $J_4$  and  $J_5$  from Ref. 6, and define the  $J_3$  to be the  $\text{Mn}^{4+}$ - $\text{Mn}^{3+}$  superexchange interaction through pyramidal base corners, and  $J_4$  the superexchange interaction through the pyramidal apex, as indicated in Fig. 1. We label the two different  $\text{Mn}^{4+}$  chains along the  $a$  axis I, II respectively, also following Ref. 6. The magnetic structure of  $R$  can be obtained from  $L$  by shifting chain II to the right (or to the left) by one unit cell along the  $a$  axis [6].

The calculated structural parameters for the structure  $L$  are listed in Table I, comparing with the experimental data, whereas the structure  $R$  is a mirror image of  $L$  about  $ac$ -plane. The calculated structural parameters are in extremely good agreement with the experimen-

TABLE II: Comparison of the  $\text{Mn}^{3+}$  positions in  $Pbam$  symmetry and  $Pb2_1m$  symmetry.

$Pbam$		$Pb2_1m$	
h	( $x, y, 1/2$ )	b(1)	( $x, y, 1/2$ )
h	( $-x+1/2, y+1/2, 1/2$ )	b(1)	( $-x+1/2, y+1/2, 1/2$ )
h	( $x+1/2, -y+1/2, 1/2$ )	b(2)	( $x+1/2+\delta x, -y+1/2-\delta y, 1/2$ )
h	( $-x, -y, 1/2$ )	b(2)	( $-x-\delta x, -y-\delta y, 1/2$ )

tal data. The errors of lattice constants are about 1%, typical errors for GGA. The atom positions are also extremely close to what was obtained experimentally. However, the small atomic displacements lower the structural symmetry to the long searched  $Pb2_1m$  polar group. To see how this happen, we take  $\text{Mn}^{3+}$  ions as an example. In the  $Pbam$  structure,  $\text{Mn}^{3+}$  has one Wyckoff position (h in Wyckoff notation) that has four equivalent sites shown in Table II. However, in the  $Pb2_1m$  structure, it splits into two Wyckoff positions b(1), b(2), each has two equivalent sites.  $\delta x$  and  $\delta y$  in Table II denote the atomic displacements from the high symmetry positions along the  $a$  and  $b$  axes respectively. The displacements along the  $a$  axis are of mirror symmetry, whereas the displacements along the  $b$  axis are not, allowing polarizations. The atomic displacements can be easily calculated from Table I. We see that the displacements are extremely small, usually are of the order of  $\sim 10^{-4}$  of the lattice constants and the largest atom displacements come from  $\text{Mn}^{3+}$ ,  $\delta y \sim 10^{-3}$  of the lattice constants. Therefore the low symmetry structure can not be directly determined experimentally, and only the anomalies of the atomic displacement parameters (ADPs) were observed [6]. We also artificially construct a high symmetry structure by symmetrizing structure  $L$  and  $R$  according to the  $Pbam$  symmetry, which we refer as structure  $H$  in the following discussions.

The calculated density of states (DOS) of structure  $L$  (and also  $R$ ) is shown in Fig.2. The DOS for spin-up and spin-down electrons is identical as expected for an AFM state. The DOS exhibits a small but clear band gap (about 0.4 eV), confirming the experimental fact that  $\text{TbMn}_2\text{O}_5$  is an insulator. However, it is well known that GGA greatly underestimates the band gap, especially for the 3d compounds. The local magnetic moments are estimated for  $\text{Mn}^{3+}$  to be  $\sim 2.37 \mu_B$ , and for  $\text{Mn}^{4+}$  to be  $\sim 1.64 \mu_B$ , in good agreement with the refined magnetic moments [6].

One of the strong evidences suggesting that the low temperature structure of  $\text{TbMn}_2\text{O}_5$  has space group  $Pb2_1m$  is that some Raman active modes become also IR active [10] at low temperature, which is forbidden by higher  $Pbam$  symmetry. To clarify this problem, we analyze the zone-center phonons. The symmetry analyses are performed on the 32-atom primitive cell [18]. For the high symmetry structure ( $Pbam$ ), the total 96 modes, are

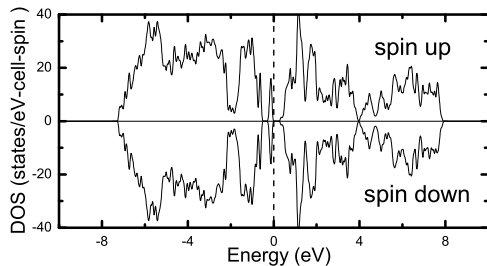


FIG. 2: The total DOS for  $\text{TbMn}_2\text{O}_5$  of structures  $L$  and  $R$ . The dashed line indicates valence-band maximum.

decomposed into 8 irreducible representations (irreps):

$$\Gamma = B_{1u} \oplus B_{2u} \oplus B_{3u} \oplus A_g \oplus B_{1g} \oplus B_{2g} \oplus B_{3g} \oplus A_u. \quad (1)$$

Among them  $B_{3u}$ ,  $B_{2u}$  and  $B_{1u}$  modes are IR active, polarized along the  $a$ ,  $b$  and  $c$  axes, respectively.  $B_{1g}$ ,  $B_{2g}$ ,  $B_{3g}$  and  $A_g$  modes are Raman active while  $A_u$  modes are silent. As we see, the Raman- and IR-active modes do not couple. However, the real crystal structure possesses a  $Pb2_1m$  symmetry, whose 96 phonons can be decomposed into 4 irreps:

$$\Gamma = A_1 \oplus B_1 \oplus B_2 \oplus A_2. \quad (2)$$

We found all modes are Raman active, among them  $A_1$ ,  $B_1$  and  $B_2$  are also IR active, and are polarized along the  $b$ ,  $c$ , and  $a$  axes respectively [10]. Detailed analyses show that the  $A_1$  modes are coupled from the  $A_g$  and  $B_{2u}$  modes. We then calculate the phonon frequencies via a frozen-phonon technique [18], as well as the oscillator strengths for the IR modes [19]. The calculated phonon frequencies are all in good agreement with the experiments, generally within  $20 \text{ cm}^{-1}$  from the experimental values. All phonons are found to be stable, i.e., no soft phonon has been found as in traditional ferroelectrics. In this letter, we show only the  $b$ -axis-polar  $A_1$  phonons in Table III, with frequencies and their oscillator strengths. To make a good contact with experiments, we divide the phonons into two presentations  $A_g$  and  $B_{2u}$  according to their major symmetry character. The experimental frequencies of the  $A_g$  phonons are extracted from Raman spectra [20], while the  $B_{2u}$  phonon frequencies are extracted from IR spectra [10]. The overall calculated oscillator strengths of  $A_1$  modes are in good agreement with the experimental values [10]. More importantly, the  $693 \text{ cm}^{-1}$   $A_g$  Raman mode, that was found also IR active with oscillator strength  $S_\lambda=0.001$  in the experiment [10], is well reproduced in the calculations, with oscillator strength  $S_\lambda=0.004$ , therefore, confirming that the ground state structure is indeed of  $Pb2_1m$  symmetry.

TABLE III: Calculated phonon frequencies ( $\omega$ ) and oscillator strengths ( $S_\lambda$ ) of IR-active  $A_1$  modes compared with experimental values. The modes are divided into  $B_{2u}$  and  $A_g$  representations according to their major symmetry character. The experimental values of  $B_{2u}$  modes are taken from Ref. 10, whereas those of  $A_g$  modes are taken from Ref. 20.

GGA		Exper.		GGA		Exper.	
$B_{2u}$				$A_g$			
$\omega$	$S_\lambda$	$\omega$	$S_\lambda$	$\omega$	$S_\lambda$	$\omega$	$S_\lambda$
100.7	0.11	97.2	0.42	110.1	0.005		
158.0	0.44	168.9	0.46	136.9	$\sim 0$		
162.8	0.50	171.9	0.30	221.6	0.009	215	
224.8	0.24	222.2	0.11	235.1	0.011	221	
267.3	0.12	256.8	0.17	312.5	0.022	334	
316.7	0.82	333.4	0.17	340.2	0.011	350	
351.3	0.09	386	0.02	405.6	0.0006	412	
412.5	0.13	422.3	0.28	445.1	0.125		
439.5	4.81	453.2	3.43	489.2	0.013	500	
471.0	1.23	481.8	2.86	529.2	0.005	537	
533.5	0.27	538.2	0.25	612.0	$\sim 0$	621	
549.3	0.12	567.3	0.52	613.5	0.0003	631	
625.0	0.36	636.6	0.27	673.6	0.004	693 <sup>a</sup>	0.001
667.2	0.009	688.3	0.003				

<sup>a</sup>experimentally observed IR active and  $703 \text{ cm}^{-1}$  measured by Aguilar et al.[10]

We next calculate the spontaneous polarization in the compound using the Berry-phase theory of polarization implemented in VASP [21]. The *intrinsic* polarization in this material is calculated to be  $1187 \text{ nC}\cdot\text{cm}^{-2}$  along the  $b$  axis. This value is an order of magnitude smaller than that of the traditional ferroelectrics. e.g.,  $\text{BaTiO}_3$ , yet it is about 30 times larger than the *currently* measured experimental value ( $\sim 40 \text{ nC}\cdot\text{cm}^{-2}$  [5]) for this compound. The large discrepancy between calculated and experimental polarizations might come from the approximations we used in the calculations. For example, we approximate the magnetic propagation vector  $k_z=0.32$  by zero. We also ignore the spin-orbit coupling and assuming collinear spins. Without these approximations, the polarization might be smaller. On the other hand, the experiment [5] measured polycrystalline samples, in which grains polarize along different directions, canceling each other, therefore might greatly underestimated the *intrinsic* polarization. We believe a high quality single crystal sample should enhance the measured electric polarization.

To further elucidate the origin of the polarization, we also calculate the spontaneous polarization for the high symmetry structure  $H$  and get  $\mathbf{P}=228 \text{ nC}\cdot\text{cm}^{-2}$ . In this case, the crystal structure has  $R^{-1}$  symmetry, however, because the special spin configuration (see Fig. 1) of the  $\text{Mn}^{3+}$ - $\text{Mn}^{4+}$ - $\text{Mn}^{3+}$  chains along the  $b$  axis breaks the  $R^{-1}$  and the combined spatial inversion and time reversal  $[(RT)^{-1}]$  symmetry of the magnetic structure, the electron wavefunctions have lower symmetry than the lattice, resulting in polarization. The *electronic* symmetry

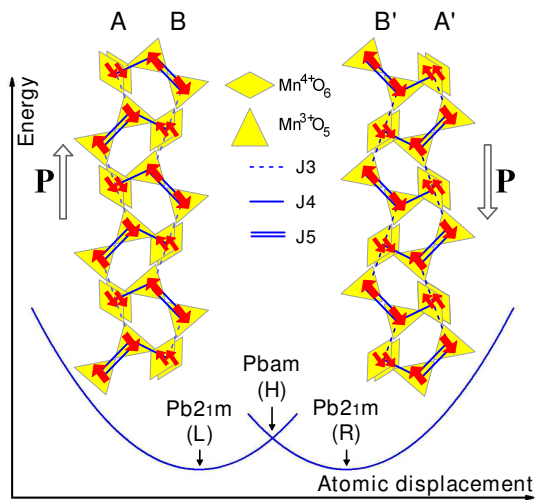


FIG. 3: (Color online) An asymmetric-spin-chain model showing the sketch of energy surfaces of structure  $L$  and  $R$  vs. the atomic displacements from the high symmetry structure. The diamonds and triangles denote the  $\text{Mn}^{4+}\text{O}_6$  octahedra and  $\text{Mn}^{3+}\text{O}_5$  pyramids respectively.

breaking will further couple to the lattice and lead to lattice distortion. Therefore, when holding atoms fixed at the centrosymmetric structure, turning on the magnetic order does two things: it generates a purely electronic polarization of  $228 \text{ nC}\cdot\text{cm}^{-2}$ , and it also applies forces to the atoms. These forces give rise to atomic displacements that yield an additional  $959 \text{ nC}\cdot\text{cm}^{-2}$ .

We now discuss the microscopic mechanism of the coupling between magnetic order and lattice. Figure 3 depicts the energy surfaces of the structure  $L$  and  $R$  vs. atomic displacements. The two structures degenerate in energy at the high symmetry structure  $H$  ( $Pbam$ ). The magnetic structures of  $L$  and  $R$  can be simplified as  $\text{Mn}^{3+}\text{-Mn}^{4+}\text{-Mn}^{3+}$  segments linked along the  $b$  axis via  $J_5$ . Inside the segments,  $\text{Mn}^{3+}$  interact with  $\text{Mn}^{4+}$  via exchange interaction  $J_3$ . In each segment, the  $\text{Mn}^{3+}$  ions above and below  $\text{Mn}^{4+}$  ions have opposite spins. For structure  $L$ ,  $\text{Mn}^{4+}$  always has the *same* sign of spin with the lower  $\text{Mn}^{3+}$ , but *opposite* sign with the upper one in each segment, whereas the opposite is true for structure  $R$ . In the high symmetry structure  $H$ , the  $\text{Mn}^{3+}$  and  $\text{Mn}^{4+}$  ions with the same sign of spin could move closer to each other to minimize the exchange energies[8]. The formal description of the coupling between the spin and the lattice is given by [1, 19]

$$-\sum_{ij\lambda} \frac{\partial J_{ij}}{\partial u_\lambda} u_\lambda \mathbf{S}_i \cdot \mathbf{S}_j, \quad (3)$$

where  $J_{ij}$  is the exchange interaction between the magnetic moments  $\mathbf{S}_i$ ,  $\mathbf{S}_j$  of the  $i$ -th and  $j$ -th atoms, and  $u_\lambda$  is the  $\lambda$ -th zone-center phonon calculated for structure  $H$ . This term is not zero, provides the magnetic struc-

ture (spin configuration)  $\{\mathbf{S}_i\}$  does not have the  $R^{-1}$  and the  $(RT)^{-1}$  symmetry, as e.g., in  $\text{TbMn}_2\text{O}_5$ . Therefore the high symmetry structure  $H$  is an unstable point on the energy surface as illustrated in Fig. 3. The structure will spontaneously relax to  $L$  or  $R$  according to the spin configuration at the high symmetry point. Furthermore, as long as the asymmetric spin structures of the  $\text{Mn}^{3+}\text{-Mn}^{4+}\text{-Mn}^{3+}$  chains are persevered, the propagation vector  $k_z$  will not change the essential physics in this system [22] which justify our approximation of setting  $k_z=0$ .

To conclude, we have shown via a first-principle study on  $\text{TbMn}_2\text{O}_5$ , how the ferroelectricity is driven by the non-centrosymmetric magnetic ordering, without invoking the spin-orbit coupling and non-collinear spins. We believe that this work sheds new light on the fundamental mechanism of the giant magnetoelectric coupling in the multiferroics, especially for the manganese oxides. Surprisingly, the calculated *intrinsic* polarization in  $\text{TbMn}_2\text{O}_5$  is as large as  $1187 \text{ nC}\cdot\text{cm}^{-2}$ , much larger than previously thought for this type of compound. The mechanism revealed here also provides useful guidance for searching for novel magnetoelectric materials.

L.H. would like to thank D. Vanderbilt for valuable suggestions. This work was supported by the Chinese National Fundamental Research Program 2006CB921900, the Innovation funds and ‘‘Hundreds of Talents’’ program from Chinese Academy of Sciences.

- 
- [1] M. Fiebig, J. Phys. D: Appl. Phys. **38**, R123 (2005).
  - [2] N. A. Hill, J. Phys. Chem. B **104**, 6694 (2005).
  - [3] T. Kimura, T. Goto, H. Shintani, K. Ishizaka, T. Arima, and Y. Tokura, Nature **426**, 55 (2003).
  - [4] T. Goto, T. Kimura, G. Lawes, A. P. Ramirez, and Y. Tokura, Phys. Rev. Lett. **92**, 257201 (2004).
  - [5] N. Hur, S. Park, P. A. Sharma, J. S. Ahn, S. Guha, and S.-W. Cheong, Nature (London) **429**, 392 (2004).
  - [6] L. C. Chapon, G. R. Blake, M. J. Gutmann, S. Park, N. Hur, P. G. Radaelli, and S. W. Cheong, Phys. Rev. Lett. **93**, 177402 (2004).
  - [7] G. R. Blake, L. C. Chapon, P. G. Radaelli, S. Park, N. Hur, S.-W. Cheong, and J. Rodriguez-Carvajal, Phys. Rev. B **71**, 214402 (2005).
  - [8] S.-W. Cheong and M. Mostovoy, Nature Materials **6**, 13 (2007).
  - [9] I. Kagomiya, S. Matsumoto, K. Kohn, Y. Fukuda, T. Shoubu, H. Kimura, Y. Noda, and N. Ikeda, Ferroelectrics **286**, 889 (2003).
  - [10] R. ValdesAguilar, A. B. Sushkov, S. Park, S.-W. Cheong, and H. D. Drew, Phys. Rev. B **74**, 184404 (2006).
  - [11] H. Katsura, N. Nagaosa, and A. V. Balatsky, Phys. Rev. Lett. **95**, 057205 (2005).
  - [12] I. A. Sergienko and E. Dagotto, Phys. Rev. B **73**, 094434 (2006).
  - [13] J. A. Alonso, M. T. Casais, M. J. Martinez-Lope, J. L. Martinez, and M. T. Fernandez-Diaz, J. Phys.: Condens. Matter **9**, 8515 (1997).
  - [14] J. P. Perdew, K. Burke, and M. Ernzerhof, Phys. Rev.

- Lett. **77**, 3865 (1996).
- [15] G. Kresse and J. Hafner, Phys. Rev. B **47**, R558 (1993).
  - [16] G. Kresse and J. Furthmuller, Phys. Rev. B **54**, 11169 (1996).
  - [17] P. E. Blochl, Phys. Rev. B **50**, 17953 (1994).
  - [18] L. He, J. B. Neaton, M. H. Cohen, D. Vanderbilt, and C. C. Homes, Phys. Rev. B **65**, 214112 (2002).
  - [19] C. Wang, G-C Guo, and L. He, *unpublished*.
  - [20] B. Mihailova, M. M. Gospodinov, B. Guttler, F. Yen, A. P. Litvinchuk, and M. N. Iliev, Phys. Rev. B **71**, 172301 (2005).
  - [21] R. D. King-Smith and D. Vanderbilt, Phys. Rev. B **47**, 1651 (1993).
  - [22] P. Radaelli and L. Chapon, arXiv:cond-mat/0609087 (2006).